ICAS-98-1,4,1

Effect of Main Rotor Configuration and Propulsion System Dynamics on Helicopter Handling Qualities

G. Guglieri * F.B. Quagliotti †
Politecnico di Torino
Dipartimento di Ingegneria Aeronautica e Spaziale
Torino - Italy

Abstract

The main objective of this paper is the study of the influence of propulsion system on the handling qualities of an articulated and a hingeless rotor helicopter in straight flight. The configuration selected is representative of a typical medium-size helicopter.
Validation results of the basic helicopter simulation model are also presented.
The mathematical model used in this study is a nonlinear blade element type model (the coupled flap-lag dynamics of each blade is modeled) that includes rotor, fuselage, main rotor inflow, actuators and propulsion system dynamics.
The additional model of propulsion system includes the contributions of engine-rotor inertial coupling and shaft torsional stiffness.
Results are provided for transfer functions, poles, bandwidths and delays at different airspeeds. The attention is focused on longitudinal, lateral and heave response, in order to evaluate the effects of propulsion system dynamics on flying qualities and prescribed ADS-33 parameters.

Notation

C_T	Thrust coefficient
e	Hinge offset
g	Acceleration due to gravity
I_{ii}	Aircraft moment of inertia
I_{ij}	Aircraft product of inertia
m	Helicopter mass
n_b	Number of blades
p, q, r	Angular velocities (body axes)
R_{2k}	Blade lag reaction acting on the hinge
TPI	Politecnico di Torino
$\mathbf{x}$	State vector
$\mathbf{u}$	Control vector
u, v, w	Velocity components (body axes)
β	Flap angle of main rotor blade
δ	Control input
ζ	Lag angle of main rotor blade
λ	Total inflow (hub axes)
θ_o	Collective pitch of main rotor
θ_{1c}, θ_{1s}	Cyclic pitch components
θ_{TR}	Collective pitch of tail rotor
μ	Advance ratio
ϕ, θ, ψ	Fuselage attitudes, Euler angles
ψ_b	Rotor hub angular displacement
ψ_1	Shaft angular displacement at the exit of the gearbox
σ	Main rotor solidity
Ω	Main rotor angular velocity
Ω_1	Shaft angular velocity
$\dot{()}$	Time derivative

Introduction

Severe torsional oscillations in the helicopter rotor drive shaft, and dynamic interface problems involving rotor, drive train and airframe subsystems have been observed in several testing conditions [1]. In this degraded operating condition, handling qualities are compromised.
The dynamic coupling of engine with fuel control and rpm-governor units is an additional critical aspect of the same problem for turbine powered helicopter.
As a matter of fact, the coupled rotor/engine/fuel control system dynamics [10] is dominated by responses in two frequency ranges: a low frequency mode of operation that characterizes the fastness of the engine speed response to fuel control inputs, and the higher frequency modes associated with the

*Assistant Professor, Member AIAA/AHS/AIDAA
†Associate Professor, Member AIAA/AIDAA

21st ICAS Congress
13-18 September 1998
Melbourne, Australia

torsional dynamics of the drive train coupled with blade lag motion.
Therefore, the design of modern helicopter engine/fuel control systems is based on both the maximization of the responsiveness of the low frequency mode and the stabilization of the higher frequency drive system dynamics. Unfortunately, the need for high control system gains, that enhance the quickness of helicopter engine response, may compromise the stability of the drive system torsional modes. Stabilization of the drive system torsional dynamics is usually obtained by correcting the size of lead lag dampers for articulated rotors or by adding a notch filter in the fuel control system. A comprehensive presentation of these aspects is given in Ref. [10].

These arguments support the research activity in the field of mathematical modeling, with the aim of extending the accuracy of simulations, that may assess the impact of engine/drive train dynamics on the operational effectiveness of the aircraft.

High fidelity models for the engine dynamics have been developed. This approach is accurate but the computational workload is generally incompatible with a high order model for rotor and airframe dynamics. These nonlinear computer simulations become inadequate for the analysis of helicopter handling qualities requirements when an extremely simplified model of rotor/airframe dynamics is adopted.
Differently, simulations may be based on a linearized state space representation of the high order mathematical model of the specific propulsion system. Linear equations are evaluated at several engine operating points, enough to cover the range of interest. Analytical or numerical interpolation is required for the current operating point.
Nevertheless, a high order validated model of the propulsion system is always necessary and the extension to different engine/drive train configurations is not straightforward.
Examples of detailed propulsion system models are given in Ref. [11, 12].

An alternative approach to the problem of modeling the effects of propulsion system dynamics on handling qualities is proposed in Ref. [9]. Drive train torsional dynamics is described by discrete masses and a flexible rotor shaft. This simplified formulation is extremely general and it was found to be accurate for the estimation of the dominant first torsional mode, which is the most important for the integration of engine and airframe. Evidence

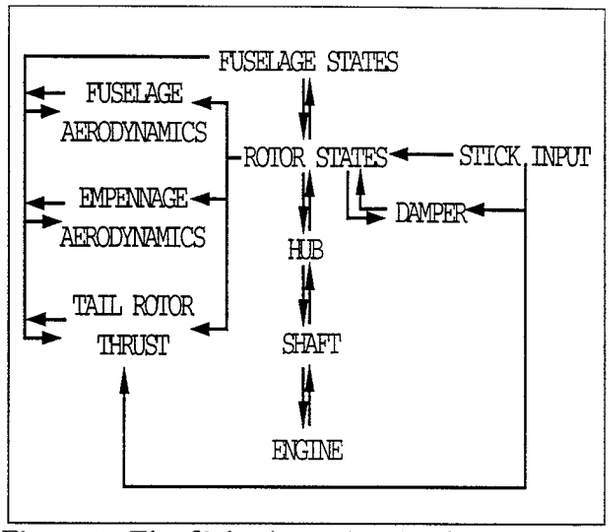

Figure 1: The flight dynamics simulation model.

is also given in Ref. [9] that decoupling the effects of engine/drive train dynamics, neglecting the rotor speed degree of freedom, is a crude approximation of the complete aircraft dynamics.
In the present paper, this last model is included in a high order validated mathematical model of rotor and helicopter airframe. The effect of the additional states on the dynamic response to control inputs is analyzed.

Mathematical Model

The mathematical model developed at TPI is a nonlinear blade-element type representation of a single rotor helicopter with rigid fuselage (see Fig. 1).
The analysis of short term response to control inputs in coordinated turns presented in Ref. [19] was based on a previous model implementation for a different helicopter, that is here extended for validation purposes.

The main rotor blades are individually modeled as rigid bodies and the coupled flap-lag dynamics is included. The equations of motion of the rotor are formulated and solved in a rotating coordinate system.
No small angle assumption is invoked for aerodynamic angles of rotor and fuselage.

The profile aerodynamic loads are calculated using two-dimensional blade element theory with table lookup for blade twist and lift/drag coefficients. An empirical formulation [7] for blade twist due to torsional dynamics is adopted.

The reactions generated by the lag dampers are nonlinear functions of the axial velocity of the damper itself. These forces are obtained following the procedure described in [7, 13].

The aerodynamics of fuselage and stabilizers is modeled using coefficients derived from wind tunnel data.

A three-state dynamic inflow model [3] is used for the main rotor.

The rigid body motion of the aircraft is modeled using six nonlinear force and moment equations and three kinematic relations:

1. Force equilibrium along body axes:

$$\begin{aligned} X &= m\,(\dot{u} + q\,w - r\,v) + m\,g\,\sin\theta \\ Y &= m\,(\dot{v} + r\,u - p\,w) - m\,g\,\sin\phi\cos\theta \\ Z &= m\,(\dot{w} + p\,v - q\,u) - m\,g\,\cos\phi\cos\theta \end{aligned}$$

2. Moment equilibrium about body axes:

$$\begin{aligned} L &= I_{xx}\,\dot{p} - I_{xy}(\dot{q} - p\,r) - I_{xz}(\dot{r} + p\,q) \\ &\quad + (I_{zz} - I_{yy})q\,r - I_{yz}(q^2 - r^2) \\ M &= I_{yy}\,\dot{q} - I_{xy}(\dot{p} - q\,r) - I_{yz}(\dot{r} + p\,q) \\ &\quad + (I_{xx} - I_{zz})p\,r + I_{xz}(r^2 - p^2) \\ N &= I_{zz}\,\dot{r} - I_{xz}(\dot{p} - q\,r) - I_{yz}(\dot{q} + p\,q) \\ &\quad + (I_{yy} - I_{xx})p\,q - I_{xy}(p^2 - q^2) \end{aligned}$$

3. Relationships between aircraft angular rates and Euler angles:

$$\begin{aligned} p &= \dot{\phi} - \dot{\psi}\sin\theta \\ q &= \dot{\theta}\cos\phi + \dot{\psi}\sin\phi\cos\theta \\ r &= \dot{\psi}\cos\phi\cos\theta - \dot{\theta}\sin\phi \end{aligned}$$

The heading rate $\dot{\psi}$ is assumed to be constant for trim analysis only.

The forces (X,Y,Z) and the moments (L,M,N) depend on the blade motion and provide the main source of coupling between the rotor and the fuselage. They also contain contributions from fuselage, tail rotor and other aerodynamic surfaces.

Both the dynamic and the aerodynamic rotor-fuselage couplings are included in the model. The latter type of coupling is typically due to the interaction of the rotor wake with the fuselage and tail surfaces, and to the changes of rotor inflow due to the presence of the fuselage.

The most important feature of the set of equations of motion for the fuselage used in the present study is that the fuselage states need not to be small quantities; thus, all the kinematic nonlinearities associated with the motion of the fuselage are retained.

The propulsion system model is a slightly modified version of that used by Chen [9], consisting of discrete masses and a flexible rotor shaft. The equation for engine/drive train torque equilibrium is:

$$I_{eq}\ddot{\psi}_1 + B_1 r_g^2 \dot{\psi}_1 + K_S(\psi_1 - \psi_b) = r_g Q_E \qquad (1)$$

where, as in Ref. [9], B_1 is the engine damping, I_{eq} is the moment of inertia of the propulsion system, referred to the rotor speed, K_S is the torsional stiffness of the rotor shaft, Q_E is the engine torque, and r_g is the nominal ratio engine/rotor speed. The equation for shaft equilibrium is:

$$I_{hub}\ddot{\psi}_b - K_S(\psi_1 - \psi_b) = \sum_{k=1}^{n_b} e \cdot R_{2k} \qquad (2)$$

where I_{hub} is the moment of inertia of the hub. This formulation is slightly more general than that of Ref. [9], which focused on specific rotor modes in which the blades moved in lag only, and with identical angular displacements. The forcing torque is obtained by summing the force contributions R_{2k} of each blade in the hub plane and perpendicular to the root segment of the blade, multiplied by the hinge offset moment arm e.

The order of the complete system is 32 and the state vector $\mathbf{x}$ can be represented as:

$$\mathbf{x} = \begin{Bmatrix} \mathbf{x_F} \\ \mathbf{x_R} \\ \dot{\mathbf{x}}_\mathbf{R} \\ \mathbf{x_I} \\ \mathbf{x_E} \end{Bmatrix} \qquad (3)$$

The vector $\mathbf{x_F}$ contains the fuselage degrees of freedom and is defined as

$$\mathbf{x_F} = [u\,v\,w\,p\,q\,r\,\theta\,\phi\,\psi]^T \qquad (4)$$

The vectors $\mathbf{x_R}$ and $\mathbf{x_I}$ include the rotor and inflow degrees of freedom, transformed in a body-fixed reference system:

$$\mathbf{x_R} = [\beta_o\,\beta_{1c}\,\beta_{1s}\,\beta_{N/2}\,\zeta_o\,\zeta_{1c}\,\zeta_{1s}\,\zeta_{N/2}]^T \qquad (5)$$

and

$$\mathbf{x_I} = [\lambda_o\,\lambda_s\,\lambda_c]^T \qquad (6)$$

Finally, the vector $\mathbf{x_E}$ refers to the engine and drive train states:

$$\mathbf{x_E} = [\psi_1 \, \Omega_1 \, \psi_b \, \Omega]^T \tag{7}$$

where $\Omega = \dot{\psi}_b$ and $\Omega_1 = \dot{\psi}_1$.
The control vector $\mathbf{u}$ is defined as:

$$\mathbf{u} = [\theta_o \, \theta_{1s} \, \theta_{1c} \, \theta_{TR} \, \dot{\theta}_o \, \dot{\theta}_{1s} \, \dot{\theta}_{1c} \, \dot{\theta}_{TR}]^T \tag{8}$$

The presence of time derivatives in $\mathbf{u}$ is required for a correct modeling of the lag dampers.

The effect of the primary pitch control actuators is also included in the mathematical model and their dynamic response is represented by a second order transfer function [13].

The trim procedure is the same as in [15]. Thus, the rotor equations of motion are transformed into a system of nonlinear algebraic equations using a Galerkin method (10 eqns.). The algebraic equations enforcing force and moment equilibrium (9 eqns.), the additional kinematic equations (2 eqns.) that must be satisfied in forward flight (or in a turn), and the momentum inflow equations for both main and tail rotor (3+1 eqns.) are added to the rotor equations, and the combined system (25 eqns.) is solved simultaneously. The solution yields the harmonics of a Fourier series expansion of the rotor degrees of freedom, the pitch control settings, trim attitudes and rates of the entire helicopter, and main and tail rotor inflow.
Flight without sideslip is arbitrarily assumed for $\mu \leq 0.1$, while roll attitude is set to zero for higher airspeed.
The propulsion system is not included in the trim process. This implies two assumptions. The first is that the engine can generate a sufficient torque in any flight condition. The second is that the small fluctuations of rotor speed associated with the lag dynamics of the rotor do not affect the engine torque.

A linearized set of small perturbation equations can be extracted from the nonlinear model:

$$\dot{\mathbf{x}} = [\mathrm{A}] \cdot \mathbf{x} + [\mathrm{B}] \cdot \mathbf{u} \tag{9}$$

The coefficients of the model are derived numerically about the trim condition, using finite difference approximations. The linearization of the rotor equations is carried out in the rotating coordinate system. A multiblade coordinate transformation (i.e. a modal coordinate transformation that is limited to the rotor degrees of freedom) converts the linearized state matrices to a fixed frame [4, 13]. Hence, the state vector $\mathbf{x_R}$ contains the components of the generalized flap coordinates in the fixed system (similar relationships apply for the lag degrees of freedom):

$$\beta_o = \frac{1}{n_b} \sum_{i=1}^{n_b} \beta_i \tag{10}$$

$$\beta_{1c} = \frac{2}{n_b} \sum_{i=1}^{n_b} \beta_i \cdot \cos \psi_{b\,i} \tag{11}$$

$$\beta_{1s} = \frac{2}{n_b} \sum_{i=1}^{n_b} \beta_i \cdot \sin \psi_{b\,i} \tag{12}$$

$$\beta_{N/2} = \frac{1}{n_b} \sum_{i=1}^{n_b} \beta_i \cdot (-1)^i \tag{13}$$

This transformation only partially reduces the periodicity of the system. Therefore, an averaging of the linearized coefficients evaluated at several positions along the blade azimuth is required.

The response to pilot inputs is obtained from direct numerical integration of the equations of motion. Note that the program is designed for off-line simulation only.
The time response to fuel flow inputs is also reproduced with a simplified approach. The increase of the turbo-shaft steady power output P_{WR} with fuel mass flow rate $\dot{m}_b$ is obtained assuming that the engine fuel control and the rpm-governor are disabled:

$$\begin{aligned} P_{WR} &= (\dot{m} + \dot{m}_b) \, \eta_{mt} \, L_T - \frac{\dot{m} \, L_C}{\eta_{mc}} \\ &= \frac{\Omega}{\eta_{tr}} \sum_{k=1}^{n_b} e \cdot R_{2k} \end{aligned}$$

where η_{mt}, η_{mc} and η_{tr} are the efficiencies of the engine/drive train components. The specific works per unit mass flow rate L_T (expansion work) and L_C (compression work) are computed using an iterative procedure with the assumption that the engine thermodynamic states change instantaneously. The comparison of vertical accelerations in hover with Ref. [9] confirms that the time response to a fuel step input is correctly predicted (Fig. 11).

Rotor speed	27 rad/s
Rotor disc radius	8.177 m
Blade m.a.c.	0.527 m
Rotor hinge offset e	0.381 m / 4.66 %
Blade Lock number γ	8.25
$n_{b_{MR}}/n_{b_{TR}}$	4
Tail rotor speed	124.62 rad/s
Tail rotor radius	1.676 m
Tail rotor m.a.c.	0.247 m
Gross weight	71211 N
CG station / waterline	8.915 m / 5.880 m
I_{XX}	6316 Kgm^2
I_{YY}	52214 Kgm^2
I_{ZZ}	49888 Kgm^2
I_{ZX}	2551 Kgm^2
K_S	541065 Nm/rad
I_{eq}	1673 Kgm^2
I_{hub}	164 Kgm^2

Table 1: The helicopter configuration.

Results

The medium size tactical utility helicopter adopted for the numerical simulations is extensively described in [7, 8]. This aircraft is a single rotor helicopter (Tab. 1) with articulated flap and lag hinges.

A hingeless rotor configuration is also considered, that is modeled with a different hinge offset (e = 12.5%) and root springs, selected so as to achieve fundamental natural frequencies in flap and lag of 1.125/rev and 0.7/rev respectively.

The flight condition correspond to an altitude of 5250 ft in standard atmosphere ($C_T/\sigma \approx 0.081$). These are the same conditions of the flight test data presented in Ref. [5].

The dynamic response is computed with stability augmentation and flightpath stabilization disabled. The stabilator positions are held fixed at trim setting determined by the numerical computations presented in Ref. [5].

In all the Bode plots, the units for angular rates and accelerations are deg/s and g, respectively, and the swashplate pitch settings are converted into inches of pilot stick input.

A general validation of static trims and frequency domain results for the basic helicopter without propulsion system dynamics is initially presented.

Next, the effects of main rotor configuration are discussed, and, finally, propulsion system dynamics is included in simulations for both articulated and hingeless rotor helicopter.

Static Trim in Forward Flight and Frequency Domain Validation

Level flight trims were obtained for airspeeds from 0 to 160 knots. Figures 2 - 5 present a comparison of calculated trim results with flight test and Ames-Genhel simulations [5]. These reference results refer to the basic helicopter with articulated rotor. Trim data for the equivalent hingeless configuration introduced in the present analysis are also included.

The agreement between the TPI predictions for the basic helicopter and the reference data is quite good for all airspeeds.

Both numerical results under predict the collective and lateral pitch settings, and the required main rotor power [5, 14] at lower airspeeds, as a consequence of the simplified model of main rotor inflow and downwash impingement on the fuselage.

The TPI simulations only under predict collective and longitudinal pitch settings for airspeeds exceeding 100 knots. This discrepancy is related with the modeling of profile aerodynamics, which, differently from Ames-Genhel, is not corrected for tridimensional effects.

Fuselage attitudes are accurately reproduced, while pedal positions are over predicted by the numerical results. A nearly constant pedal bias to the right is calculated by Ames-Genhel and the TPI code. The reference flight test data for pedal positions are supposed to be inaccurate at low speeds, as explained in Ref. [5].

The on-axis frequency responses in hover for the two main rotor configurations are shown in Figures 6 - 9. Engine dynamics is disabled (i.e. $\Omega = \Omega_1$) and the order of the system is reduced to 28 states.

A comparison is presented with the results generated by the Ames-Genhel code, through system identification techniques [6]. The frequency band for which this nonlinear identification process may be considered accurate is slightly wider than $[1 \div 10]$ rad/s. These reference numerical results were also successfully compared with other simulations and flight tests in Ref. [13, 16].

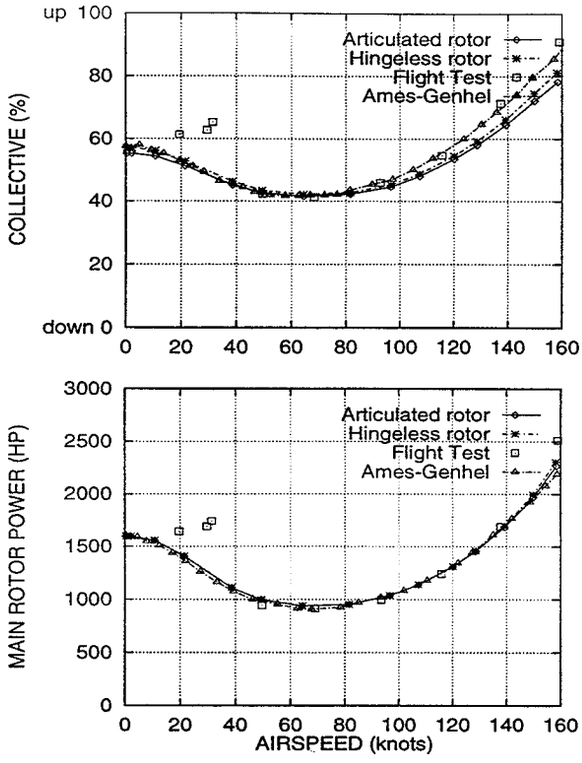

Figure 2: Collective pitch and required main rotor power at trim.

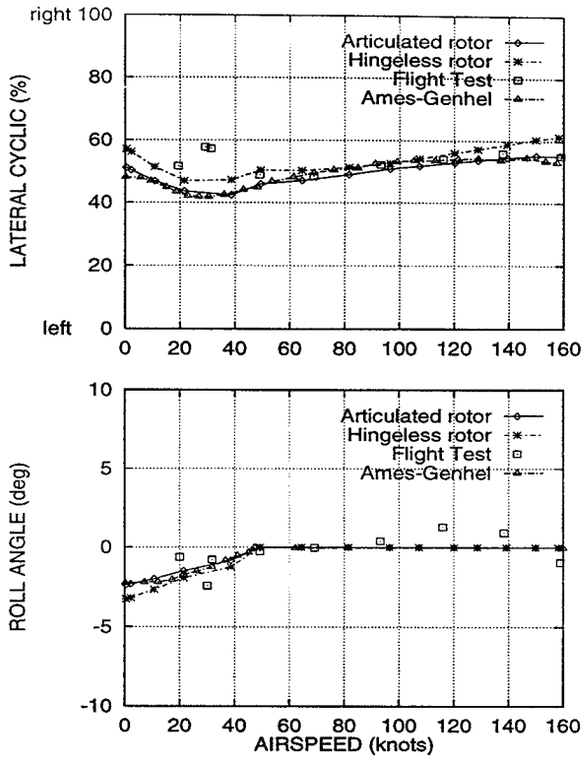

Figure 4: Lateral cyclic and fuselage roll attitude at trim.

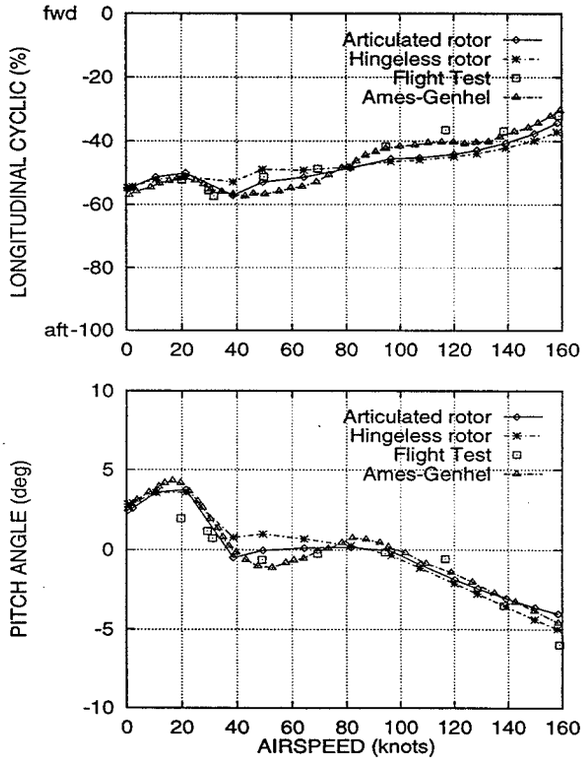

Figure 3: Longitudinal cyclic and fuselage pitch attitude at trim.

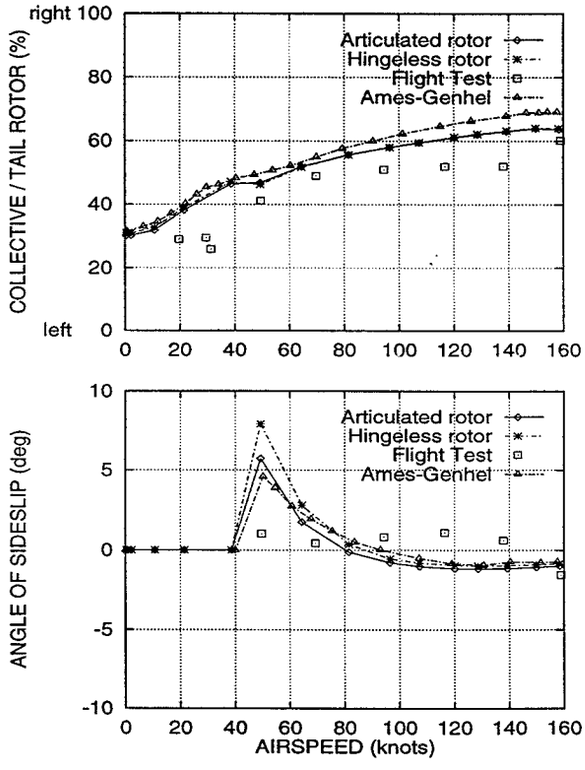

Figure 5: Pedal position and fuselage sideslip angle at trim.

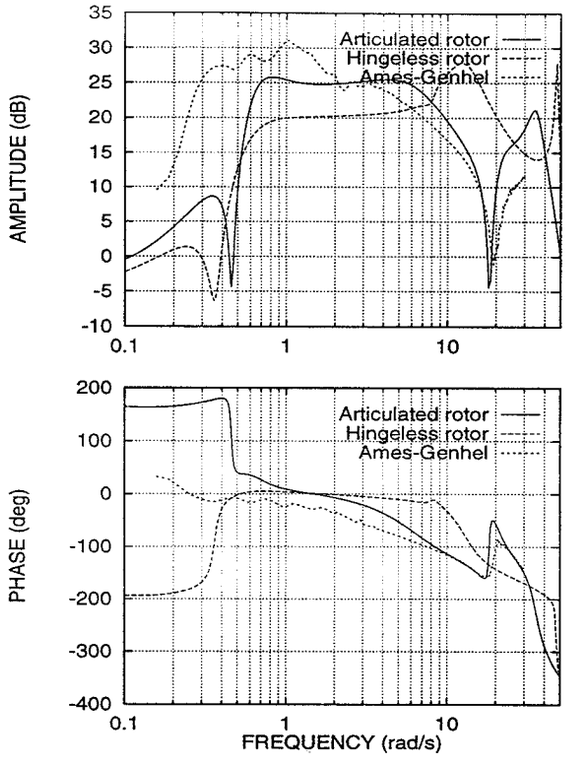

Figure 6: Bode plots of roll rate response to lateral cyclic pitch input in hover.

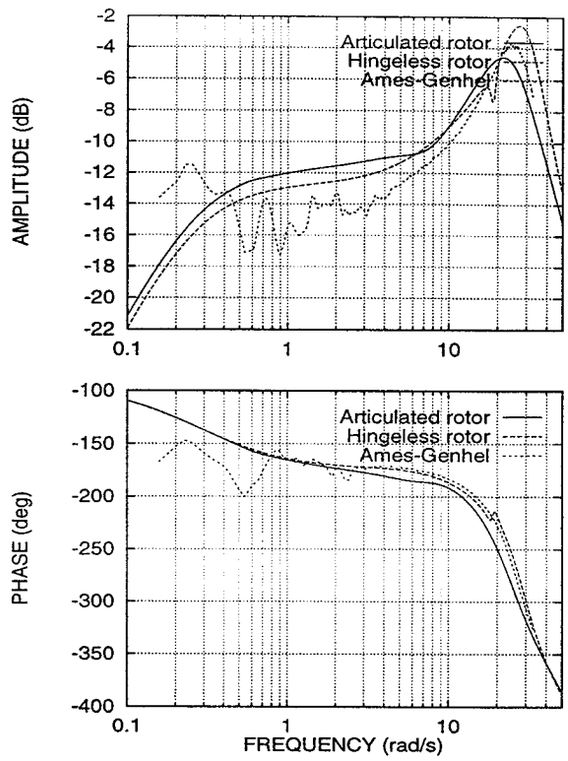

Figure 8: Bode plots of vertical acceleration response to collective pitch input in hover.

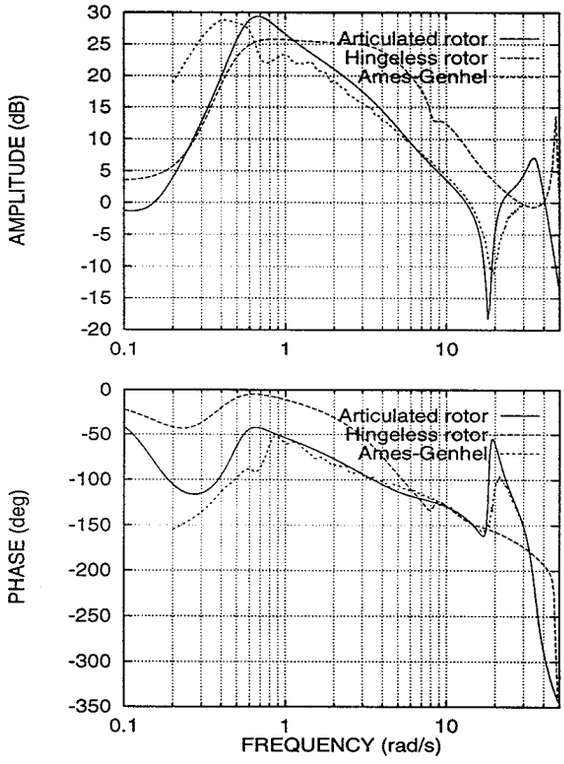

Figure 7: Bode plots of pitch rate response to longitudinal cyclic pitch input in hover.

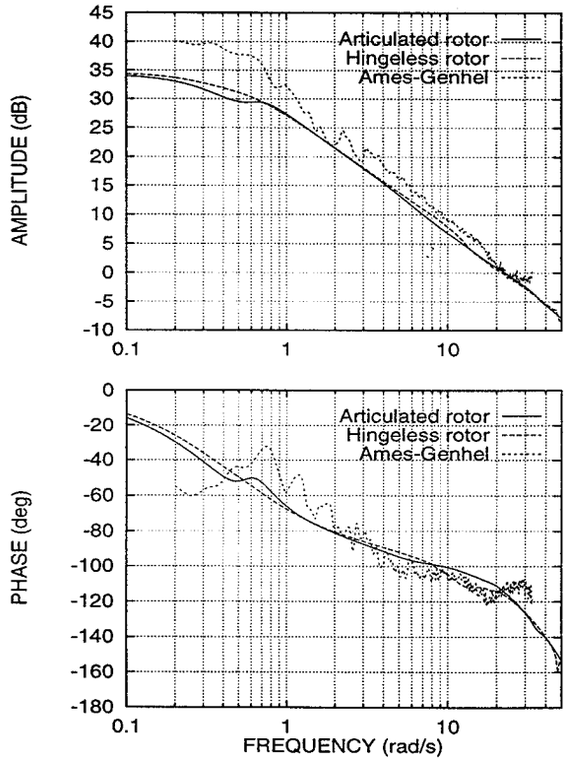

Figure 9: Bode plots of yaw rate response to pedal input in hover.

Note that propulsion system dynamics is included in Ames-Genhel simulations [7], although the rotating shafts of the drive train are assumed to be torsionally rigid.
With the aim of validating the TPI frequency responses, the attention is initially focused on the data obtained for the basic articulated rotor.

The trend of the roll rate response to lateral cyclic input for the articulated rotor is comparable with the reference data for the frequency band over 5 rad/s. At lower frequencies, moderate discrepancies appear in magnitude and phase, although below 0.5 rad/s and above 10 rad/s no conclusive estimation of the accuracy of the numerical simulations can be made, due to the low coherence of the reference data. At higher frequencies, the TPI code correctly reproduces the main rotor dynamics, matching the notch response linked with the regressive lag mode (damping ratio $\zeta = 0.179$ and natural frequency $\omega_n = 19.808\,\text{rad/s}$).

The Bode plot of pitch rate response to longitudinal cyclic pitch input is presented in Fig. 7. The correlation between the results for the articulated rotor and the reference numerical data is good, within the frequency range of acceptable coherence for the Ames-Genhel nonlinear identification process.

The vertical response $\dot{w}$ to collective input (Fig. 8) evaluated with the TPI code is substantially comparable with the previous numerical simulations, although gains are moderately over predicted in the low frequency range.

Finally, the trend of the yaw rate response to pedal input is correctly reproduced by TPI data in Fig. 9.

Effects of Main Rotor Configuration

Trim data for the hingeless rotor are substantially comparable with the results obtained for the reference articulated configuration (see Fig. 2 - 5).

Poles were identified by comparing frequencies and eigenvectors for the two different main rotor configurations in hovering flight, without engine dynamics. Damping ratios and natural frequencies are presented in Tab. 2 and Fig. 10:

- inflow dynamics: main rotor inflow modes are stable and highly damped for both configurations;
- flap dynamics: flap modes depend on rotor configuration, and the articulated rotor exhibits a natural frequency for the fundamental flap mode $\omega_F = 1/\text{rev}$, while the root spring for the hingeless blade was selected so as to achieve $\omega_F = 1.125/\text{rev}$;
- lag dynamics: the natural frequency of the fundamental lag mode is sensitive to the rotor configuration ($\omega_L = 0.26/\text{rev}$ and $\omega_L = 0.7/\text{rev}$ respectively);
- fuselage dynamics: the analysis of eigenvectors demonstrates that these modes are coupled with rotor states for both main rotor configurations, and a moderate instability is found for the forward speed/pitch mode (phugoid).

	articulated rotor		hingeless rotor	
mode	ζ (-)	ω_n (rad/s)	ζ (-)	ω_n (rad/s)
inflow	0.9754	31.152	0.9960	27.168
inflow	1.0000	16.333	1.0000	13.492
$1+\omega_F$	0.2248	49.447	0.1608	54.996
ω_F	0.4884	26.254	0.3288	30.083
ω_F	0.4382	24.128	0.3008	29.382
$1-\omega_F$	0.5991	6.238	0.2694	12.876
$1+\omega_L$	0.1062	35.600	0.0142	47.480
ω_L	0.5611	7.102	0.0506	18.935
ω_L	0.5384	7.040	0.0480	18.959
$1-\omega_L$	0.1797	19.808	0.0982	8.215
roll	1.0000	5.205	0.6348	4.422
pitch	1.0000	1.584		
spiral	1.0000	0.362	1.0000	0.406
heave	1.0000	0.290	1.0000	0.280
d. r.	0.3326	0.638	0.5886	0.522
phugoid	-0.3379	0.509	-0.5073	0.453
heading	0.0000	0.000	0.0000	0.000

Table 2: The poles of the helicopter in hover.

The effect of the two different flap and lag dynamics, combined with the rotor/fuselage dynamic coupling, is also evident when comparing the Bode plots of roll (Fig. 6) and pitch rate (Fig. 7) frequency responses to command input.
Differently, heave (Fig. 8) and yaw (Fig. 9) frequency responses are marginally affected by the change of main rotor configuration.
In each case, the frequency at -135° for heave response is consistent with the value of $Z_w = 0.280 \div$

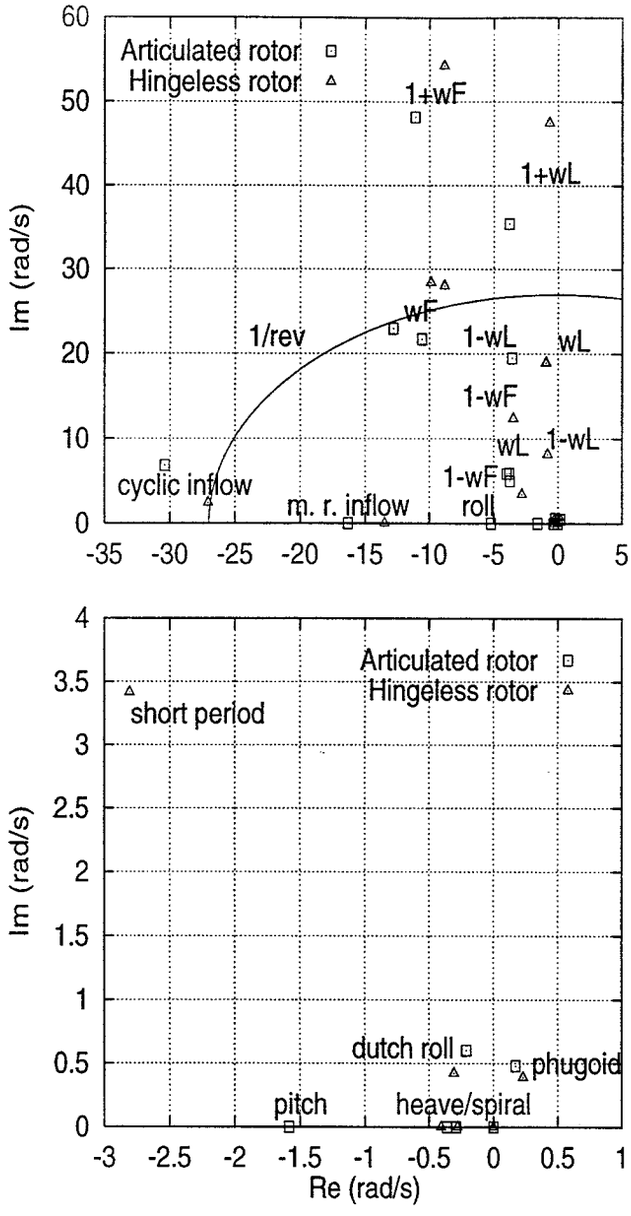

Figure 10: Poles of the helicopter in hover without engine dynamics.

$0.290\,s^{-1}$ in Tab. 2, assuming a first order transfer function for

$$G(i\omega) = \frac{\overline{w}}{\overline{\theta}_o} = \frac{Z_{\theta_o}}{i\omega - Z_w} \qquad (14)$$

Effects of Propulsion System Dynamics

The computational workload is moderately affected by the presence of the additional states related to drive train dynamics. However, propulsion system dynamics introduces intermodal couplings that complicate the identification of poles and normal modes. The related eigenvectors always include the engine variables (ψ_b, ψ_1). Furthermore, merging of the fuselage modes is also observed in some flight conditions.

	articulated rotor		hingeless rotor	
engine param.	ζ (-)	ω_n (rad/s)	ζ (-)	ω_n (rad/s)
$K_S = K_{S_o}$ $I_{eq} = I_{eq_o}$	0.2343	18.339	0.0291	18.098
$K_S \to \infty$ $I_{eq} \to \infty$	0.5626	7.102	0.0502	18.928

Table 3: The first torsional mode in hover.

Additional modes are introduced in the complete dynamic system (see also Ref. [9] for further details):

- first torsional mode: this is primarily an engine/shaft motion coupled with blade lag dynamics;
- second torsional mode: the hub motion is coupled with blade lag dynamics;
- rigid body mode: engine, hub and blades rotate as a rigid body ($\omega_n = 0$).

The first torsional mode is originated by the migration of two lead lag complex conjugate roots, and these eigenvalues migrate back to $\omega_n = \omega_L$ increasing both K_S and I_{eq} (Tab. 3). This lightly damped mode is important in engine/airframe dynamic integration [9].

As a matter of fact, the increase of shaft stiffness and equivalent engine inertia alters the imaginary parts of the two torsional poles. Anyway, the higher frequency mode (hub mode) is less sensitive to any alteration of K_S and I_{eq}.

A degradation of the system stability was also found in Ref. [18] for the first torsional mode when the shaft stiffness was substantially increased. In order to remove this numerically induced instabilities, moderate structural lag damping was introduced ($\zeta_L = 0.05$) for the hingeless rotor configuration.

The response to collective and fuel flow step was also analyzed (Fig. 11). No engine rpm governor was considered in the present model.

The rpm response is characterized by a sharp deceleration of the engine/drive train system for positive collective step. The oscillatory behavior of Ω and

Ω_1 during the initial transient of the rpm response demonstrates that the first torsional mode is excited by the command input.

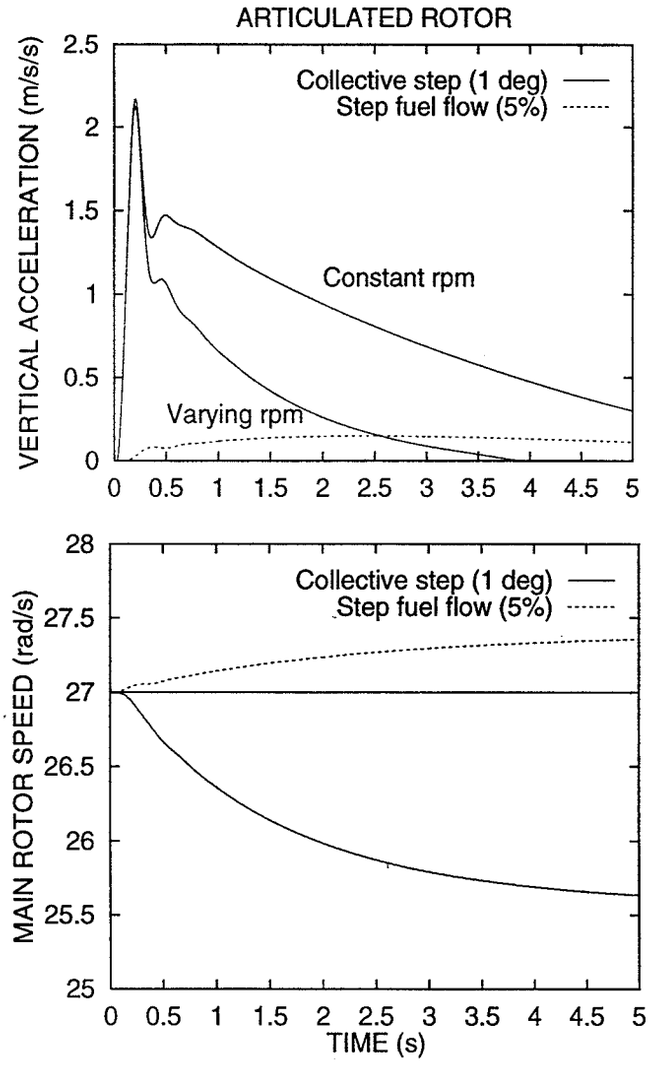

Figure 11: Vertical acceleration and rpm response to collective step and fuel flow input in hover.

The time history of vertical acceleration is substantially different when engine/drive train dynamics is included. Note that the flattened response predicted by the varying rpm model is confirmed by flight test data [9].

The rate of climb responses in hover (Fig. 12) show that the articulated rotor exhibits higher vertical damping (about 4% without engine/drive train dynamics and 12% including rpm variation). As a consequence, the hingeless rotor in hovering flight presents higher time constants for heave response.

The inclusion of propulsion system dynamics produces a significant reduction (-70%) of the steady

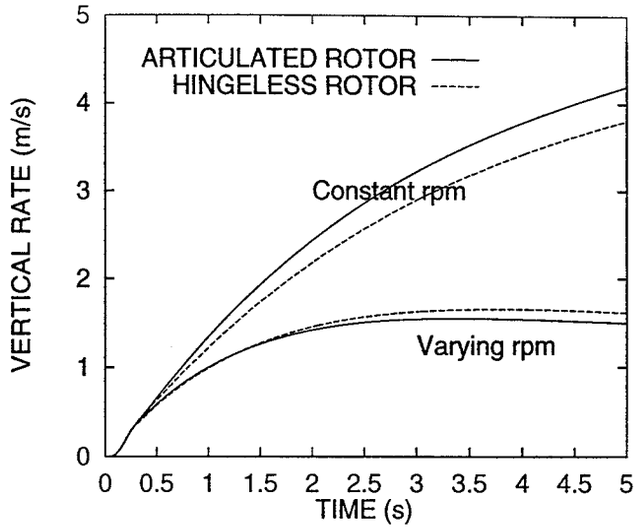

Figure 12: Vertical rate response to 1 deg collective step input in hover.

state rate of climb in hover

$$w_\infty = -(Z_{\theta_o}/Z_w) \cdot \theta_o \qquad (15)$$

related to the substantial increase of heave damping Z_w with $\dot{\Omega} \neq 0$.

The results in hovering flight also demonstrate that the collective sensitivity Z_{θ_o} is only moderately affected by the rotor configuration or by the presence of propulsion system dynamics.

Handling Qualities Criteria

The height response to collective controller was analyzed according to ADS-33 specifications (Ref. [2]). The vertical rate response must respect a first order approximation for at least 5 seconds after a step collective input:

$$\dot{h} = K \cdot \left[1 - e^{\left(\frac{t-\tau_{\dot{h}}}{T_{\dot{h}}}\right)}\right] \qquad (16)$$

where the gain K, the time constant $T_{\dot{h}}$ and the time delay $\tau_{\dot{h}}$ are to be determined with a least squares time domain regression fitting. The goodness of fit is also restricted.

As remarked in Ref. [17], the criterion specifies a collective step input, but no indication is given whether the other commands are supposed to remain fixed. The question is significant when $\dot{h}$ has not a first order appearance, as required in Ref. [2]. This may lead to numerical singularities or inaccurate estimation of the first order response parameters. Therefore, the present results were obtained

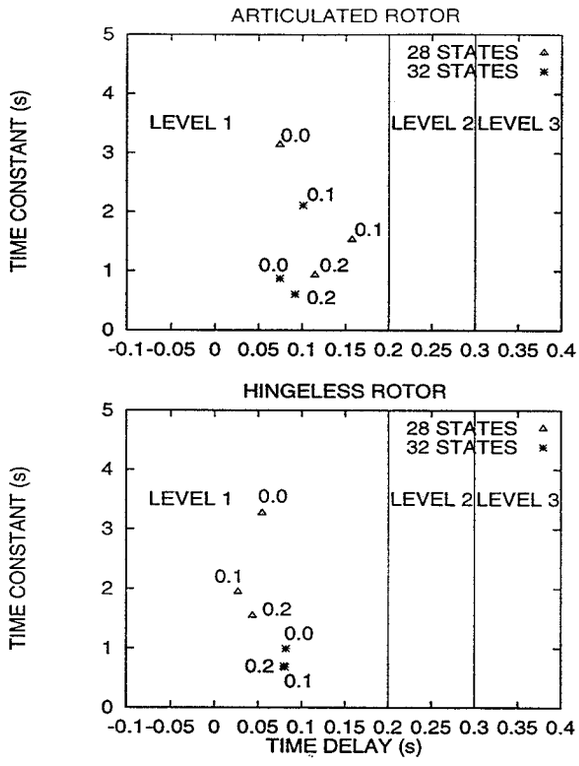

Figure 13: Time delays and time constants for vertical rate response at different advance ratios μ.

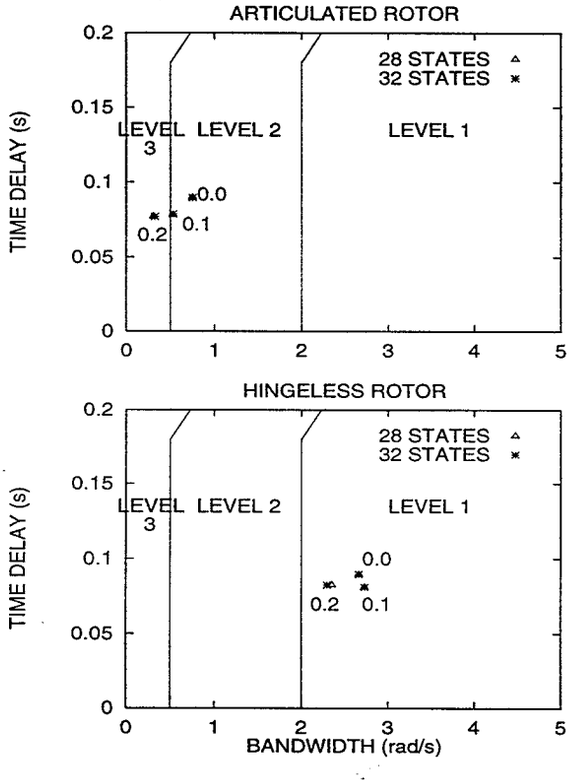

Figure 14: Pitch bandwidth and phase delay at different advance ratios μ.

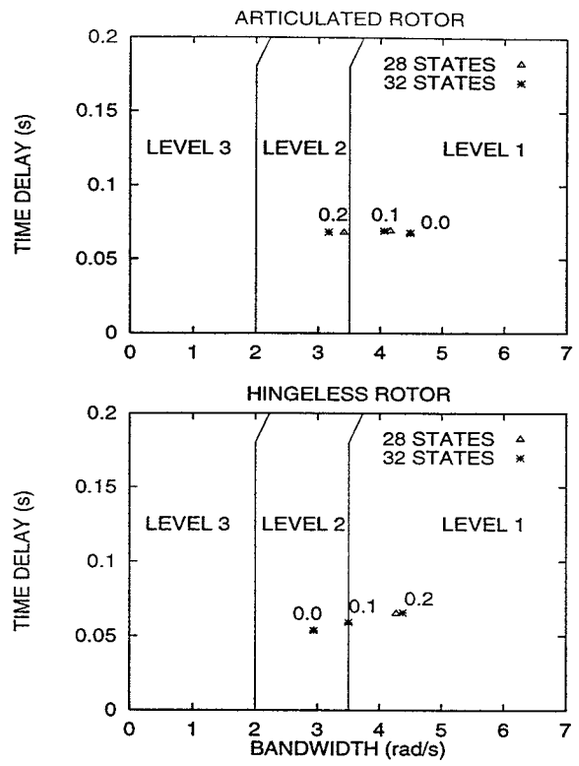

Figure 15: Roll bandwidth and phase delay at different advance ratios μ.

enabling a proportional feedback control of pitch attitude for advance ratios $\mu \geq 0.1$.

Both articulated and hingeless rotor exhibit level 1 handling qualities in forward flight (Fig. 13). Significant changes for the time constant T_h are observed between responses computed with and without engine/drive train dynamics, that affects the aircraft vertical damping.

The short term response to control input for the *Target Acquisition and Tracking* task were also analyzed with the bandwidth criteria specified in Ref. [2] for small amplitude attitude changes. The results for pitch/roll responses to longitudinal/lateral cyclic inputs are given in Fig. 14 - 15. These data were derived for an unaugmented helicopter configuration.

The hingeless rotor presents higher pitch bandwidths, within the Level 1 requirements. The articulated configuration shows Level 2 handling qualities in forward flight and a bandwidth decrease for higher airspeeds.

The two configurations have comparable Level 1 roll handling qualities, but opposite bandwidth increase with advance ratio.

The specific ADS-33 parameters for small ampli-

tude attitude changes show that pitch and roll handling qualities are not influenced by the presence of propulsion system dynamics in the mathematical model [16, 18].

Summary and Conclusions

A generalized model for engine/drive train dynamics was implemented, after the validation of the TPI mathematical model.

The first torsional mode is predicted by this simplified formulation.

Numerical experiments demonstrate that the computational workload is moderately increased by the presence of the additional states related to propulsion system dynamics.

Open loop short term pitch and roll handling qualities are unaffected by propulsion system dynamics for both main rotor configurations, while heave response is altered by shaft torsional dynamics.

References

[1] Sanders, J.C., "Influence of Rotor-Engine Torsional Oscillation on Control of Gas-Turbine Geared to a Helicopter Rotor", NACA-TN-3027, 1953.

[2] "Aeronautical Design Standard ADS-33C, Handling Qualities Requirements for Military Rotorcraft", U.S. ARMY AVSCOM Technical Report, August 1989

[3] Peters, D.A., HaQuang, N., "Dynamic Inflow for Practical Applications", J. of the American Helicopter Society, vol. 33, n. 4, 1988

[4] Johnson, W., "Helicopter Theory", Dover Publications, 1994, pp. 349-361

[5] Ballin, M.G., "Validation of a Real Time Engineering Simulation of the UH-60A Helicopter", NASA-TM-88360, Feb. 1987.

[6] Ballin, M.G., Dalang-Secretan, M.A., "Validation of the Dynamic Response of a Blade Element UH-60 Simulation Model in Hovering Flight", J. of the American Helicopter Society, vol. 36, n. 4, 1991

[7] Howlett, J.J., "UH-60A Black Hawk Engineering Simulation Program: Volume I - Mathematical Model", NASA-CR-166309, Dec. 1981

[8] Lambert, M.,, "Black Hawk, Lamps and AAH", Flight International, 25 Feb. 1978

[9] Chen, R.T.N., "An Exploratory Investigation of the Flight Dynamic Effects of Rotor RPM Variations and Rotor State Feedback in Hover", NASA-TM-103968, 1992

[10] Bielawa, R.L., "Rotary Wing Structural Dynamics and Aerolasticity - Drive System Dynamics", AIAA Education Series, pp. 133-161, 1992

[11] Duyar, A., Gu, Z., Litt, J.S., "A Simplified Dynamic Model of the T700 Turboshaft Engine", J. of the American Helicopter Society, vol. 40, n. 3, 1995

[12] Hamers, M., von Grunhagen, W., "Dynamic Engine Model Integrated in Helicopter Simulation", 23rd European Rotorcraft Forum, paper n. 91, Dresden, 1997

[13] Kim, F.D., Celi, R., Tischler, M.B., "High-Order State Space Simulation Models of Helicopter Flight Mechanics", J. of the American Helicopter Society, vol. 38, n. 4, 1993

[14] Kim, F.D., Celi, R., Tischler, M.B., "Forward Flight Trim and Frequency Response Validation of a Helicopter Simulation Model", J. of Aircraft, vol. 30, n. 6, 1993

[15] Celi, R., "Hingeless Rotor Dynamics in Coordinated Turns", J. of the American Helicopter Society, vol. 36, n. 4, 1991

[16] Kim, F.D., "Formulation and Validation of High Order Mathematical Models of Helicopter Dynamics", PhD Dissertation, Univ. of Maryland, 1991

[17] Ockier, C.J., "Flight Evaluation of the New Handling Qualities Criteria Using the BO 105", J. of the American Helicopter Society, vol. 41, n. 1, 1996

[18] Guglieri, G., Celi, R., Quagliotti, F.B., "Effect of Propulsion System Dynamics on Rotorcraft Aeromechanical Stability in Straight and Turning Flight", AGARD Symposium on Advances in Rotorcraft Technology, Ottawa, Canada, 1996

[19] Guglieri, G., Celi, R., "On Some Aspects of Helicopter Flight Dynamics in Steady Turns", J. of Guidance, Control and Dynamics, vol. 21, n. 2, 1998